

Accepted Manuscript

Title: Bimetallic gold-silver catalysts based on ZnO and Zn/SBA-15 - the effect of various treatments on surface and catalytic properties

Authors: Iveta Kaskow, Izabela Sobczak, Chia-Min Yang, Maria Ziolek



PII: S0920-5861(19)30317-7
DOI: <https://doi.org/10.1016/j.cattod.2019.06.036>
Reference: CATTOD 12283

To appear in: *Catalysis Today*

Received date: 29 October 2018
Revised date: 25 May 2019
Accepted date: 11 June 2019

Please cite this article as: Kaskow I, Sobczak I, Yang C-Min, Ziolek M, Bimetallic gold-silver catalysts based on ZnO and Zn/SBA-15 - the effect of various treatments on surface and catalytic properties, *Catalysis Today* (2019), <https://doi.org/10.1016/j.cattod.2019.06.036>

This is a PDF file of an unedited manuscript that has been accepted for publication. As a service to our customers we are providing this early version of the manuscript. The manuscript will undergo copyediting, typesetting, and review of the resulting proof before it is published in its final form. Please note that during the production process errors may be discovered which could affect the content, and all legal disclaimers that apply to the journal pertain.

Bimetallic gold-silver catalysts based on ZnO and Zn/SBA-15 - the effect of various treatments on surface and catalytic properties

Iveta Kaskow^{1,2}, Izabela Sobczak^{*1}, Chia-Min Yang^{**2,3}, Maria Ziolek¹

¹Adam Mickiewicz University in Poznan, Faculty of Chemistry, Uniwersytetu Poznańskiego 8, 61-614 Poznan, Poland

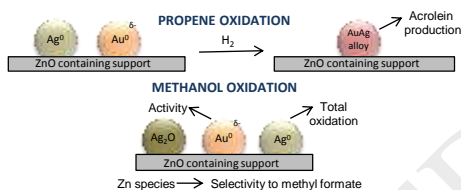
²Department of Chemistry, National Tsing Hua University, Hsinchu 30013, Taiwan

³Frontier Research Centre on Fundamental and Applied Sciences of Matters, National Tsing Hua University, Hsinchu 30013, Taiwan

*Corresponding author: sobiza@amu.edu.pl

**Co-corresponding author: cmyang@mx.nthu.edu.tw

Graphical abstract



Highlights

- Thermal treatment of AuAg-SBA-15 in inert gas and H₂ flows led to alloy formation.
- Au-Ag alloy favoured the selectivity towards acrolein in propene oxidation with O₂.
- Silver species were responsible for activity in propene total oxidation.
- Gold (Au⁰)^{δ-} was responsible for the activity in methanol oxidation with O₂.
- Zinc favoured deeper degree of alloying and selectivity to methyl formate.

Abstract

Two different supports containing zinc (ZnO and Zn/SBA-15) were used to prepare mono- and bimetallic gold, silver and gold-silver catalysts. Zinc was used for two different purposes in these materials: (i) as a support in the form of zinc oxide and (ii) as a dopant introduced to short-channel SBA-15 by wetness impregnation. Short channel SBA-15 was used as the reference support. The materials obtained were characterized by: N₂ physisorption, XRD, TEM, UV-Vis, XPS, XAS and their activity was tested in the reactions of propene and methanol oxidation in the gas phase. The state of metals (Au, Ag, Zn) and the composition of gold-silver alloy formed on the catalysts surface were considered in terms of thermal activation of catalysts in inert gas and in hydrogen flow as well as interaction with reagents and products of methanol and propene oxidation. It was found that silver species were responsible for the activity in propene oxidation and its total combustion to CO₂, whereas (Au⁰)^{δ-} metallic particles were active in methanol oxidation. Selectivity to acrolein in propene oxidation was achieved thanks to the presence of Au-Ag alloy whose composition depended on the presence of zinc oxide and activation conditions. The alloy was not stable and separated into metals upon propene oxidation conditions. In methanol oxidation, zinc species took part in selective oxidation to methyl formate.

Keywords: gold, silver, ZnO, platelet SBA-15, Zn/SBA-15, propene and methanol oxidation

1. Introduction

It is well known that the activity of gold catalysts depends on many factors like the size of gold crystallites, the type of support, interactions of metal with the support as well as other components of the catalyst (dopant, second metal: Ag, Cu, Pt, Pd) [1,2]. Strong metal-support interaction (SMSI) may modify structural, electronic and catalytic properties of gold [3]. The strength of interaction is greater when metal oxide instead of silica is applied as the support. The interaction between gold and silica is strengthened by the addition of metal dopant to the support [4]. Also the addition of a second metal usually improves electronic properties and catalytic activity of gold, which is a result of the synergetic effect between both

metals [2,5]. It was shown that due to a low ability of gold to activate oxygen, the addition of silver can positively influence gold activity in oxidation reactions. As reported in [2] Au-Ag systems belong to the Au-BM (BM=metals like Ag, Cu, Ni) group of catalysts in which BM show good properties in promoting activated oxygen in oxidation reactions which are as well catalysed by gold. According to literature data [6,7], gold-copper catalysts based on silica were shown as promising, active and selective catalyst for the production of acrolein from propene by selective oxidation using a mixture of H_2 and O_2 as oxidant. To the best of our knowledge, there is no report on the activity of gold-silver catalysts in propene oxidation with molecular oxygen. Partial oxidation of propene over Au-Ag alloy using electrochemical oxygen provided via voltage application has been presented in [8]. However, the reaction pathway with the use of electrochemical oxygen is different than that with participation of molecular oxygen in the reaction performed on supported Au-Ag catalyst surface.

In our recent papers [9,10], Au-Cu and Au-Ag catalysts supported on mesostructured cellular foams (AuAg-NbMCF, AuCu-Zn/MCF) have been found to show high activity in methanol oxidation with high selectivity to formaldehyde as a result of synergetic interactions between metals.

In this work we studied the activity of two groups of mono (Au and Ag)- and bimetallic (Au-Ag) catalysts containing zinc in the support (ZnO and Zn/SBA-15 as the supports) in the two above mentioned processes: oxidation of propene and methanol in the gas phase. In both groups of catalysts zinc played different roles. In ZnO-based catalysts, zinc oxide was used as the support, whereas in Zn/SBA-15 based samples, zinc oxide dispersed on mesoporous silica played the role of a support dopant.

Zinc oxide is widely used in different areas of industry for example as a gas sensor or photocatalyst in degradation of harmful substances [11]. Mou and co-workers [12] have shown that the strong metal-support interactions (SMSI) occurred between ZnO support and

gold crystallites. They have reported the presence of two different SMSI. Upon treatment in oxygen at 573 K, O-SMSI were obtained and characterized by the transfer of electrons from gold to the support. R-SMSI were achieved in the reduction conditions and high temperature (573 K) leading to the electron transfer from the support to gold. Both effects can be reversed when the conditions are changed (oxygen atmosphere to hydrogen and vice versa).

SMSI can be achieved also when ZnO is dispersed on an inert support. SBA-15 is a popular inert support often used in catalysis as it has large surface area, thick walls, its pore diameter can be tuned and it shows hydrothermal stability. On the other hand, because of the long mesochannels, such a support can generate a problem with molecular diffusion and pore blockage during catalytic reactions [13,14]. This problem can be avoided by the use of the platelet SBA-15 containing short mesochannels (~200 nm). To obtain platelet SBA-15, small amount of Zr(IV) ions is introduced to the reaction mixture as they increase the rate of the Pluronic P123 and TEOS self-assembly [15].

The main focus of this paper was to study the effect of zinc in ZnO and Zn/SBA-15 which support metals and various treatments of catalysts on the metals-support interaction and the surface and catalytic (propene and methanol oxidation) properties of gold, silver- and gold-silver catalysts. Moreover, the role of zinc was estimated by a comparison with the performance of catalysts based on silica (SBA-15). Particular attention was paid to the role of Au-Ag alloy, its formation and participation in oxidation processes studied.

2. Experimental

2.1. Chemical compounds

The compounds used were zinc acetate (anhydrous, Aldrich, >99.00 %), Pluronic P123 ((ethylene glycol)₂₀-(propylene glycol)₇₀-(ethylene glycol)₂₀, Aldrich), oxalic acid (Aldrich, >99,999 %), distilled water, methanol, zirconyl chloride (ZrOCl₂ x 8H₂O, Acros

Organics), tetramethoxysilane (TMOS, Alfa Aesar), chloroauric acid ($\text{HAuCl}_4 \times 4\text{H}_2\text{O}$, Johnson Matthey - UK-USA), hydrochloric acid (Showa Chemical Co. Ltd), sulphuric acid (Showa), zinc nitrate ($\text{Zn}(\text{NO}_3)_2$, Aldrich) (3-Mercaptopropyl)trimethoxysilane (Aldrich, 95%), dry toluene (POCH, $\geq 99.8\%$), sodium borohydride (Aldrich, $\geq 98\%$), silver nitrate (AgNO_3 , Aldrich). The above chemical compounds were not purified before use.

2.2. Supports synthesis

Zinc oxide was obtained according to the following procedure: 8.57 g of anhydrous zinc acetate was dissolved at RT (295 K) in an appropriate amount of water (71 mL) and Pluronic P123 (7.4 g) was dissolved in 71 mL of methanol. These two solutions were stirred for one hour. Meanwhile water-methanol (71 mL of H_2O , 71 mL of MeOH) solution of acetic acid (4.2 g) was prepared and added dropwise to the mixture of zinc acetate and P123. Obtained precipitate was filtered and washed with water and methanol, then dried at 333 K. The final product was obtained by calcination at 723 K for 4 hours [16].

SBA-15 with short channels was prepared according to the procedure described in [15,17] in the following steps: 8 g of Pluronic P123 with zirconyl chloride (1.32 g) were stirred overnight (308 K) in a mixture of distilled water (250 mL) and hydrochloric acid (44 mL, 35%). After that, 12.4 g of TMOS was quickly added and the mixture was kept at 308 K for 24 hours. After that, sulphuric acid (11.6 mL, 98%) was added and the mixture was stirred for 1 minute. Then the mixture was kept at 363 K without stirring. After 24 hours the product was filtered and washed with distilled water and a small amount of acetone. Obtained solid was dried at 333 K and calcined at 813 K.

2.3. Impregnation of SBA-15 with zinc nitrate

To obtain Zn/SBA-15, SBA-15 silica was subjected to the incipient wetness impregnation with a water solution of $\text{Zn}(\text{NO}_3)_2 \times 6\text{H}_2\text{O}$. Then it was sonicated for 20 minutes, dried at 353 K and calcined at 773 K for 4h. The zinc loading was 6 wt. %.

2.4. Functionalization with (3-Mercaptopropyl)triethoxysilane (MPTMS)

Eight grams of the support (ZnO, Zn/SBA-15, SBA-15) were added to a mixture of dry toluene (200 mL) and MPTMS (20 mL). The mixture was heated under reflux for 18 hours at 383 K. Then it was filtered and washed with toluene (200 mL), ethanol (200 mL), water (100 mL) and dried at 353 K.

2.5. Modification of the functionalized supports with Au and/or Ag

The supports were modified by the method proposed by Mou and co-workers [18]. Water solution of HAuCl_4 as a metal precursor (2.2 wt. % of Au as assumed) was stirred for 1 hour at room temperature with an appropriate amount of the functionalised support. After filtration and washing with distilled water, the solid was stirred for 20 minutes with water solution of NaBH_4 (0.1 M) in order to reduce the cationic gold. The solid product was recovered by filtration and washing. For obtaining monometallic Ag samples, AgNO_3 (2.2 wt. % of Ag as assumed) was used as a metal precursor and the whole procedure was repeated as for gold.

For the preparation of bimetallic Au-Ag catalysts, the step by step method was used. At first gold (2.2 wt. % as assumed) was introduced to the support by the procedure described above and then silver (0.7 wt. % as assumed) was incorporated in the same way. The final materials were obtained by drying at 373 K and calcination at 773 K for 4 h.

2.6. Catalyst characterization

The synthesized materials were characterized by the following methods: N₂ physisorption, XRD, UV-Vis, TEM, SEM, XPS and XAS.

2.6.1. N₂ physisorption

N₂ physisorption isotherms were obtained at 77 K Using a Quantachrome Autosorb iQ apparatus. All samples were pre-treated in situ under vacuum at 573 K. The BET method was used to calculate the surface area of the catalysts and BJH method was applied to estimate the pore volume and diameter.

2.6.2. X-Ray Diffraction (XRD)

XRD analysis of the samples was performed on a D8 Advance diffractometer (Bruker). CuK α radiation ($\lambda = 0.154$ nm) was used and the step size was of 0.05° in the $2\theta = 6-60^\circ$ range.

2.6.3. Ultraviolet Visible Spectroscopy (UV-Vis)

UV-Vis spectra were recorded using Varian-Cary 300 Scan (ZnO based materials) and JASCO V-650 (SBA-15 based materials) spectrophotometers. A small amount of the catalyst was transferred into a cell equipped with a quartz window. Measurements were performed at ambient temperature in the wavelength range from 800 to 190 nm. Spectralon was used as a reference material.

2.6.4. Transition Electron Microscopy (TEM)

For transmission electron microscopy (TEM) measurements, Philips EM-400 (ZnO based materials) and JOEL JEM-2100 (SBA-15 based materials) electron microscopes were used to get the information on the size of metal crystallites. A small amount of the sample was deposited on the carbon-coated grid and then transferred to the microscope.

The sizes of metal crystallites were estimated from TEM images by measuring about 100 particles on the images and plotting crystallite sizes distribution. The standard deviation of these measurements was calculated from the formula:

$$S = [\sum (d_i - d_{av})^2 / \sum n_i]^{1/2}$$

where: n_i – number of crystallites measured, d_i – size of the indicated crystallite, d_{av} – mean crystallite size.

2.6.5. Scanning Electron Microscopy (SEM)

Field emission JEOL JSM-7000 F microscope operating at 10 kV equipped with an energy-dispersive X-ray spectrometer (EDX) was used to obtain SEM images.

2.6.6. X-ray Photoelectron Spectroscopy (XPS)

X-ray photoelectron spectroscopy (XPS) was performed in VG MKII ESCALAB (ZnO based materials) and ULVAC-PHI XPS: PHI Quantera SXM (SBA-15 based materials) photoelectron spectrometers with Al $K\alpha$ radiation. VG MKII ESCALAB Spectrometer was equipped with concentric hemispherical electron energy analyser, pass energy used was 20 eV. In the case of ULVAC-PHI XPS: PHI Quantera SXM a spherical capacitor analyser and channel detector were used.

2.6.7. X-ray absorption spectroscopy (XAS)

The XAS data were recorded at the National Synchrotron Radiation Research Center in Taiwan (NSRRC) at Au L_3 -edge at beamline 17C with a storage ring energy of 1.5 GeV and an electron beam current of 360 mA in a top-up injection mode. The IFEFFIT package with ATHENA and ARTEMIS programs were used to process the results of measurements. The energy calibration, background subtraction and normalization leading to XANES spectra extraction were used in order to process the data.

2.7. Catalytic activity

2.7.1. Propene oxidation

Catalytic activity of all catalysts was tested in the propylene oxidation in the gas phase. A portion of 0.05 g of the catalyst was transferred to the fix-bed flow reactor in which

the reaction was carried out. Before the reaction, the catalyst was pretreated with helium (40 mL/min) for 2 hours at 673 K or in hydrogen flow at 673 K for 2 hours (H₂:He= 10:30 mL/min). The reaction was run at 523 K or 573 K and the reaction mixture was composed of: propylene, oxygen and helium at a given flow rate ratio: 1.25 : 1.25 : 22.5 mL/min. Products formed during the reaction were analysed using an Agilent 7890A gas chromatography system, equipped with a Molecular sieve 5A and a Porabond Q column, each containing a thermal conductivity detector and a flame ionization detector.

The conversion of propene and the selectivity to acrolein were calculated as follows:

$$\text{Propene conversion} = \frac{(\text{moles of oxygenates} + \text{CO}_2)/3}{\text{moles of propene in feed}}$$

$$\text{Acrolein selectivity} = \frac{\text{moles of acrolein}}{(\text{moles of oxygenates} + \text{CO}_2)/3}$$

The molar fraction of each compound was determined on the basis of calibration curves.

2.7.2. Methanol oxidation

The reaction of methanol oxidation in gas phase was performed in a glass bed reactor into which appropriate amount of the material was placed (0.04 g of SBA-15 or 0.03 g of ZnO diluted with 0.03 g of SiO₂). The size of the catalysts was kept in the range between 0.5 < Ø < 1 nm. Tested samples were activated in the argon flow of 40 mL/min (2 hours, 673 K) or they were treated with hydrogen (H₂:Ar = 10:30 mL/min, 2 hours, 673 K) before the reaction. The reaction was run at four temperatures- 373 K, 423 K, 473 K and 523 K. The reaction mixture was composed of Ar/O₂/MeOH in the following ratios: 23.4/3.2/2.5 mL/min. Methanol was transported to the reactor by argon flowing through the glass saturator filled with methanol (POCH, Poland). Two gas chromatographs were used to analyse the reaction products. A chromatograph with a TCD detector, Porapak Q and 5A molecular sieves columns was used to analyse such products like: CO, CO₂, H₂O, O₂, CH₃OH. The columns were heated

according to the following programme: 5 min at 358 K, increase in the temperature to 408 K (heating rate 5 K/min), 4 min at 408 K, cooling down to 358 K (for the automatic injection on the column with 5A), 10 min at 358 K, increase in the temperature to 408 K (heating rate 10 K/min), 11 min at 408 K. To analyse organic compounds formed during the reaction, a GC 8000 TOP chromatograph equipped with a capillary column of DB-1 and (operated at 313 K) a FID detector was used. To avoid condensation of reaction products the line between the reactor and gas chromatographs was heated to 373 K. Argon was the carrier gas. For the estimation of methanol conversion the external standard was used, whereas the selectivity to products was determined by means of molar fraction of each compound calculated using the proper molar coefficients. CO₂ concentration was determined on the basis of calibration curve.

3. Results and discussion

3.1. Structural/textural properties of the supports

Two different supports, ZnO and Zn/SBA-15, were used to obtain two groups of Au and AuAg-catalysts. The catalysts supported on SBA-15 (without zinc) were used as reference materials. The structural/textural properties of the samples obtained were studied using N₂ physisorption and XRD techniques. XRD pattern of synthesized ZnO showed the hexagonal wurzite structure that is typical of zinc oxide (Fig. 1A). All the characteristic reflexes are present in the diffractogram at $2\theta = 31.8^\circ, 34.4^\circ, 36.2^\circ, 47.5^\circ, 56.6^\circ$. They correspond to the (100), (002), (101), (102), (110) planes [19]. XRD pattern of zinc oxide is in agreement with the structure of ZnO in JCPDS card No.01-089-1397. For all materials containing gold and/or silver (Au-ZnO, Ag-ZnO, AuAg-ZnO) the XRD reflexes characteristic of ZnO remained unchanged (Fig. 1A) indicating the stability of the support structure upon modification. Physisorption of N₂ was used to establish the BET surface area of ZnO-based samples (Table 1). The parent ZnO has a relatively low surface area (18 m²/g). The textural

parameters were almost the same before and after modification. Moreover, the porosity of ZnO support was poorly developed.

For SBA-15, three characteristic reflections ($\sim 2\theta = 0.9^\circ, 1.5^\circ, 1.7^\circ$) were observed in the low angle XRD pattern (Fig. 1B), corresponding to the (100), (110), (200) planes, respectively [14,15]. XRD results confirmed that the short-channel SBA-15 with 2D hexagonal $p6mm$ pore structure was successfully obtained. The platelet morphology of SBA-15 matrix was confirmed by SEM images (SD-Fig.S1). For Zn/SBA-15, a shift of XRD diffractions peaks ((110) and (200) planes) to higher 2θ characteristic of a decrease in pore size indicated ZnO was grafted inside the channels [20]. The lack of reflections characteristic of ZnO in the wide-angle XRD pattern (Fig.2C) suggests good dispersion of ZnO or the presence of amorphous ZnO, or zinc incorporation into the pore walls of SBA-15 silica.

The N_2 physisorption isotherms of SBA-15 based supports and the textural parameters of the materials are presented in Fig. S2 (SD) and Table 1. All the materials showed IV type of isotherms with H_1 hysteresis loop. Siliceous SBA-15 exhibited the largest surface area ($680 \text{ m}^2/\text{g}$). The impregnation of the mesoporous silica with zinc species caused a significant decrease in the surface area to $348 \text{ m}^2/\text{g}$. Simultaneously, a decrease in the pore volume and pore diameter was observed as a result of high loading of zinc on SBA-15 surface. The addition of metals (Au and/or Ag) resulted in further reduction of all textural parameters, but to a lower extent than the impregnation with Zn. It should be mentioned that the loading of Zn was about three times higher than that of Au and/or Ag.

3.2. The loading of metals on ZnO and Zn/SBA-15

The results of ICP analysis showing real metal loading in all samples studied are presented in Table 2. For Au-ZnO and AuAg-ZnO catalysts the real metal loading of gold was equal to the nominal one (2.2 wt. % of Au as assumed). It shows that the interaction of gold

(in the form of AuCl_4^- ions) with MP (-SH groups) functionalising moiety was conducive to gold incorporation [10,21]. For Au-SBA-15 and AuAg-SBA-15 materials the real gold content was significantly lower than the nominal value, whereas for Au-Zn/SBA-15 and AuAg-Zn/SBA-15 it showed only slight deviations from the planned metal loading (Table 2). The formation of negatively charged gold particles (Au^0) $^{\delta-}$ after reduction with NaBH_4 (documented in 3.3.3. section) allowed the following efficient introduction of cationic silver (Ag^+). The efficiency of silver introduction in monometallic catalysts depended on the type of support (ZnO vs Zn/SBA-15 and SBA-15) and it was much higher for mesoporous silica. Only 0.7 wt. % of silver was present in Ag-ZnO (2.2 wt. % of Ag as assumed), which could be explained by the fact that MPTMS used for the functionalization of the support shows lower affinity to silver than to gold. The higher loading of silver in SBA-15 based materials resulted from cation exchange on the surface of silica (the exchange of proton in silanol groups for silver cations).

3.3. The state of Au and Ag and Zn on the surface of the catalysts

XRD, TEM, UV-Vis, XPS and XAS methods were used in order to get information about the state of metals in the samples studied.

3.3.1. XRD

XRD technique gives not only important information about the structure of a material, but also about the type of metal species (metallic state, oxide). However, one should remember about its limitations, because for metal crystallites of too small size or for too low metal loading no characteristic diffraction peaks can appear. In the XRD pattern of Au-ZnO, the peak characteristic of metallic gold is not well visible (it can be hidden under the shoulder in the range at $2\theta = 38-39^\circ$), whereas for Au-SBA-15 and Au-Zn/SBA-15 two diffraction peaks at $2\theta \cong 38.0^\circ, 44.0-44.5^\circ$ appeared (Fig. 2). According to literature, the diffraction peaks

at $2\theta = 38.2^\circ$ and 44.4° are typical of metallic gold [22,23]. They are assigned to the metallic gold planes (111) and (200), respectively [5,13]. In XRD pattern of Ag-ZnO three reflections are seen (at $2\theta = 28.2^\circ$, 38.1° and 44.3°). The first should be assigned to Ag_2O in which silver is in cationic form [24]. Two other reflections at $2\theta = 38.1^\circ$ and 44.3° are attributed to metallic silver [19]. In contrast, for Ag-SBA-15 only one peak from Ag_2O was observed ($2\theta = 31.8^\circ$) [28], whereas for Ag-Zn/SBA-15 there were no reflections from silver species. The lack of reflections from metallic silver and Ag_2O in XRD patterns can be a result of a very good dispersion of silver crystallites and the presence of silver oxide on the surface of the support. Diffraction peaks at $2\theta \cong 38.5^\circ$ and 44.5° were present for all bimetallic catalysts. It should be noted that for the samples containing zinc (AuAg-ZnO and AuAg-Zn/SBA-15) these peaks were positioned at lower values ($2\theta = 38.3^\circ$ and 44.3°) suggesting interaction of noble metals with zinc species. Due to the fact that gold and silver have the same face centred cubic structures with slightly different lattice constants of 0.408 nm and 0.409 nm, respectively, it is hard to unambiguously assign these reflections to metallic gold, metallic silver or Au-Ag alloy [25,26]. Moreover, it is also impossible to identify the zinc species in Zn/SBA-15 based catalysts, because the reflections typical of ZnO (at $2\theta = 31.6^\circ$, 34.2° and 36.2°) [19] can be hidden under the broad peak from silica.

3.3.2. UV-Vis

UV-Vis spectroscopy was used as a complementary technique in order to get more information about the state of metals, their coordination and the presence of alloy. UV-Vis spectra of the catalysts studied are shown in Figure 3. All spectra showed a very intense band located in the range between 250 nm and 380 nm coming from charge transfer in ZnO [27]. In the range characteristic of noble metals (400-600 nm), the UV-Vis spectrum of Au-ZnO showed the surface plasmon resonance (SPR) band (Fig. 3A) whose maximum value was found at 521 nm. For bimetallic AuAg-ZnO the position of this band was almost the same

(520 nm) as for Au-ZnO. This band should be assigned to metallic gold, which is in agreement with literature data [28-30]. The described UV-vis spectroscopy results confirmed the XRD results. Due to the presence of the band characteristic of ZnO it is difficult to identify cationic gold (Au^+ , Au^{3+}) in the samples supported on ZnO [31]. The bands characteristic of cationic gold species should be visible in the range of 200-370 nm [31] and can be hidden under the wide band characteristic of ZnO. The UV-Vis spectra of Ag-ZnO and AuAg-ZnO catalysts did not show any bands characteristic of silver species because of the wide band from ZnO support which covered the range characteristic of these species. Thus, further investigation by XPS was necessary.

To check the stability of the surface of bimetallic catalysts after activation and reduction processes (in the conditions used before the catalytic reaction), the UV-Vis measurements were performed after the treatment of the samples with inert gas (2 hours, 673 K, Ar = 40 mL/min) and next with hydrogen (2 hours, 673 K, H_2 :Ar = 10:30 mL/min). The UV-Vis spectra indicated changes in the surface composition (Fig. 3, Table 3). After activation in the inert gas flow, the maximum of the SPR band in the spectrum of AuAg-ZnO-A (Fig. 3A) was shifted towards lower wavelengths (blue-shift) when compared with its position before the activation (from 520 to 507 nm). This behaviour indicates the formation of gold and silver alloy [26]. It has been documented earlier that the higher the silver content in the alloy, the greater the blue-shift of the UV-Vis band characteristic of metallic gold towards the band from metallic silver (at ca. 400 nm) [25]. Taking into account that the blue-shift discussed above is relatively small, it can be postulated that Au-Ag alloy formed in AuAg-ZnO-A contains a small amount of silver. Further thermal treatment of the catalyst with hydrogen led to the blue-shift of the SPR band towards lower wavelength (from 507 nm for AuAg-ZnO-A to 500 nm for AuAg-ZnO-H) indicating the enrichment of Au-Ag alloy in silver (Table 3).

Similarly, as for Au-ZnO, the band from metallic gold was found in the UV-Vis spectra of mesoporous gold-containing materials (Fig. 3B, C). However, the position of this band was different than that observed for Au-ZnO (504 and 502 nm for Au-SBA-15 and Au-Zn/SBA-15, respectively, vs 520 nm for Au-ZnO) and it did not depend on the presence of zinc on SBA-15 surface (Fig. 3C). It is known that the position of SPR band depends on the size of gold particles and their local environments [32]. The SPR band is red-shifted with increasing size of metal particles. Thus, it cannot be the case in this study because the difference in the band position is not in line with average gold particle size in Au-SBA-15 and Au-Zn/SBA-15 samples (TEM results described below). It indicates that the difference in positions of SPR maxima comes from the differences in the gold particles surroundings. On Zn/SBA-15 gold is located mainly on silica surface and partly close to ZnO on silica surface, in contrast to its location on ZnO support.

In contrast to the spectrum of calcined AuAg-ZnO, for bimetallic mesoporous catalysts (AuAg-SBA-15, AuAg-Zn/SBA-15) a smaller blue shift of the band was observed than that of band in the spectrum of monometallic gold catalysts (from 504 to 495 nm for AuAg-SBA-15 and from 502 to 498 nm for AuAg-Zn/SBA-15). It indicates the formation of Au-Ag alloy, but with very low silver content. The spectra of both monometallic silver materials (Ag-SBA-15, Ag/Zn-SBA-15) exhibited bands characteristic of metallic silver at ca. 410 nm [26], which proves that besides cationic silver (i.e. Ag₂O indicated by XRD) also metallic silver is present on the surface of the silver catalysts. For bimetallic AuAg-SBA-15-A and AuAg-Zn/SBA-15-A activated in inert gas flow (2 hours, 673 K, Ar = 40 mL/min) a blue shift of SPR band was observed relative to its position in the spectra of calcined catalysts (to 480 nm for AuAg-SBA-15-A and to 481 nm for AuAg-Zn/SBA-15-A). It indicates that Au-Ag alloy became enriched in silver after activation at 673 K. The effect of temperature activation on the alloy formation was similar for both samples (a blue-shift of SPR band

similar as in the spectra of calcined sample – Table 3). The effect of reduction treatment (673 K, 2 hours, H₂:He = 10:30 mL/min) was also observed. The position of the SPR band was shifted to 479 nm for AuAg-SBA-15-H (a shift of 1 nm) and 467 nm for AuAg-Zn/SBA-15-H (a shift of 14 nm). It is a confirmation that Au-Ag alloy with higher content of silver than in the catalyst activated in argon was formed only in AuAg-Zn/SBA-15-H [26]. It indicates that the presence of zinc favoured deeper alloying of gold and silver as a result of hydrogen treatment. Moreover, the blue-shift was higher for AuAg-Zn/SBA-15-H than for AuAg-ZnO-H (Table 3). It demonstrates that the enrichment of alloy in silver was greater when ZnO was dispersed on the surface of mesoporous silica. Thus, the interaction of small ZnO particles loaded on SBA-15 with metallic species was stronger and resulted in deeper alloying of gold and silver.

3.3.3. XANES

XAS spectroscopy was used for deeper analysis of metal oxidation states and confirmation of Au-Ag-alloy formation as a result of hydrogen treatment of AuAg-Zn/SBA-15 sample. The XANES spectra were recorded at Au L₃-edge for bimetallic catalysts (based on SBA-15 and Zn/SBA-15) after calcination, after reduction at 673 K and after reduction and treatment in the reaction conditions, they are shown in Figure S3. The spectra of both, AuAg-SBA-15 and AuAg-Zn/SBA-15 materials, looked similar to that of Au-foil (metallic gold), indicating the domination of metallic gold in calcined samples (despite the fact that UV-Vis measurements showed the presence of an alloy with a low silver content). For bimetallic samples reduced in hydrogen, a change in XANES profiles was observed (the disappearance of the band at ca. 12030 eV). This change in spectra profiles can be a result of the formation of AuAg-alloy structure documented by the UV-Vis spectroscopy results.

3.3.4. XPS

XPS analysis of all samples was performed in order to get more detailed information about the state of metals and interactions between them and the support. According to literature reports, the binding energy (BE) of metallic gold is 84.0 eV [33,34]. For all monometallic gold catalysts (Au-ZnO, Au-Zn/SBA-15, Au-SBA-15) the binding energy of Au 4f_{7/2} was ca. 83.3-83.2 eV (Table 4, Fig. S4, S5 - SD). This lower value of binding energy of gold than that of bulk Au⁰ metallic gold particles indicates that some negative charge is present in the vicinity of metallic gold particles loaded on the supports [35,36]. This kind of (Au⁰)^{δ-} species dominated in all samples (Table 4). It has been evidenced [9,18] that these gold species were formed as a result of accumulation of electrons coming from chloride ions originating from the gold source (chloroauric acid) during catalysts preparation or from nucleophilic centres on the surface of mesoporous silica, which are able to donate electrons from the support to gold particles. Besides metallic gold, also cationic gold was present in all materials (BE = ca 85.0 eV – Table 4) except for AuAg-SBA-15 [31,37]. It is important to note that Au-ZnO and Au-Zn/SBA-15 contained cationic gold species (Au^{δ+}, BE = 85.0 eV) more positively charged than those in Au-SBA-15 (Au^{β+}, β < δ, BE = 84.6 eV). It is a result of electron transfer from cationic gold to zinc in Zn-containing supports indicating the interactions between cationic gold and zinc species. The binding energy of metallic gold did not change after SBA-15 modification with zinc, which indicates the lack of (Au⁰)^{δ-}-zinc interactions. Similarly, the introduction of silver to all gold containing samples (based on ZnO, Zn/SBA-15 and SBA-15) did not change BE of metallic and cationic gold species. It means that the addition of silver did not influence the electronic state of gold (Table 4), indicating that gold-silver interaction did not occur in calcined samples. On the other hand, a decrease in binding energy typical of Zn2p_{3/2} (characteristic of Zn²⁺ bonded to the oxygen ion –Table 4) [26,38] was visible for the samples modified with gold (Au-ZnO and Au-Zn/SBA-

15). The decrease in $Zn2p_{3/2}$ BE value (from 1022.0 to 1021.5 eV for Au-ZnO and from 1022.9 to 1022.4 eV for Au-Zn/SBA-15) confirmed gold (cationic species)-zinc interaction.

Similarly, silver in monometallic catalysts based on all supports studied was present in two forms, metallic (BE of $Ag3d_{5/2} = 368.3$ eV) [19] and cationic one (BE of $Ag3d_{5/2} = 367.5-367.3$ eV) [30,39] (Table 4, Fig. S6, S7-SD). Metallic silver is well known as the species easily transferring electrons [25]. The decrease in BE characteristic of $Zn2p_{3/2}$ for samples containing silver, relative to that of $Zn2p_{3/2}$ of ZnO and Zn/SBA-15 supports (from 1022.0 to 1021.6 eV for Ag-ZnO and from 1022.5 to 1022.3 eV for Ag-Zn/SBA-15) indicates the interaction between silver and Zn in the support and the electron transfer from silver species to zinc.

3.3.5. TEM

Transition electron microscopy (TEM) was used in order to get information about the particle size distribution of the metals loaded on ZnO, Zn/SBA-15 and SBA-15. Particle size distribution diagrams based on TEM images (Fig. S8) are shown in Figure 4. The average size of gold particles for Au-ZnO and AuAg-ZnO is similar (2.8 nm and 2.9 nm, respectively). There is only a little difference in the distribution of the metal crystallites on the catalysts surface. One can conclude that the addition of silver does not influence in any specific way the size of the gold crystallites. The average size of gold particles on Au-Zn/SBA-15 is much bigger than on Au-ZnO (5.5 vs 2.8 nm). On Zn/SBA-15 gold particles are located not only in the vicinity of ZnO, but also on silica surface. The weaker interactions of gold with silica than with ZnO are the reason for higher agglomeration of metal particles on the surface of Zn/SBA-15.

Comparing the catalysts based on SBA-15, the effect of zinc on the particle size distribution is especially visible for bimetallic samples. The fraction of smaller metal particles between 3-5 nm is greater for AuAg-Zn/SBA-15 than AuAg-SBA-15. It is known from

literature [9,40] that ZnO dispersed on the support can reduce the size of gold and alloy particles by limiting aggregation of metal particles during calcination.

The hydrogen treatment of bimetallic AuAg-samples led to an increase in the average metal particles size (Table 2, Fig. S9). It is especially observed for SBA-15 materials. The majority of crystallites on mesoporous silica had diameters in the range between 6 nm and 10 nm (Fig. 5). It is clear that the reduction process favours aggregation of metal particles. The formation of Au-Ag alloy increases the size of metal particles. An increase in metal particles size with increasing silver concentration in alloy has been observed earlier for AuAg-MCM-41 catalysts [41].

3.4. Catalytic activity

3.4.1. Propene oxidation with molecular oxygen

Catalytic activity of all ZnO and SBA-15 based catalysts was tested in propene oxidation in the gas phase. In this reaction acrolein is a desired product. It is used in chemical industry as an intermediate in syntheses of other chemicals [7]. The mono- and bimetallic catalysts after activation in inert gas (A) and after treatment in hydrogen (H) were studied at the reaction temperatures 523 and 573 K. All the results are shown in Table 5.

ZnO, Zn/SBA-15 and SBA-15 supports did not show any catalytic activity at both reaction temperatures. Very low conversion of propene (up to 3% at 573 K) was observed for gold modified samples (Au-ZnO-A, Au-Zn/SBA-15-A, Au-SBA-15-A -Table 5). The highest activity was obtained for the samples modified with silver. The samples with higher silver loading (Table 2), Ag-Zn/SBA-15-A and Ag-SBA-15-A, revealed higher activity (17 % and 18 % propene conversion at 573 K, respectively) than Ag-ZnO-A (10 % conversion) which contained much less amount of silver. Thus, it is clear that silver species were responsible for propene oxidation. Metallic silver is known as the species on which the adsorption of oxygen takes place [42]. Therefore, its role in propene oxidation seems to be enhancement of activity

via chemisorption of oxygen. However, silver catalysts were active mainly in total oxidation of propene (selectivity to $\text{CO}_2 \geq 90\%$, Table 5). It is in agreement with theoretical calculations, which showed that the mechanism of total oxidation of propene over silver catalysts is energetically more favourable [42]. It has been proved that the olefins containing allylic C–H bonds (like in propene) are completely oxidized to CO_2 . The mechanism involves the reaction of allylic hydrogen with the oxygen adsorbed on the surface of silver (abstraction of an allylic hydrogen takes place). The allyl species formed is further combusted to CO_2 and H_2O in the presence of oxygen. In contrast to silver catalysts, gold containing materials were less active but more selective to acrolein.

The addition of gold to silver loaded on the supports significantly decreased the activity towards propene conversion over silver catalysts because of Au-Ag alloy formation as a result of catalyst activation in the inert gas. On the other hand, the addition of silver to gold caused an increase in activity which can be due to the presence of silver species or Au-Ag alloy. A comparison of acrolein selectivity over the samples showing almost the same activity (3 – 4 % of propene conversion) is presented in Fig. 6. If one relates selectivity to acrolein over bimetallic catalysts to the selectivity achieved over monometallic gold samples (Fig. 6A, Table 5), the higher acrolein production over bimetallic samples is clear. Acrolein production increased over bimetallic catalysts because the presence of gold-silver alloy decreased the oxygen chemisorption on silver and in this way decreased the total oxidation of propene. The effect of zinc on acrolein selectivity is presented in Fig. 6B. AuAg-ZnO-A on which Au-Ag alloy contained the smallest amount of silver (concluded from UV-Vis spectra; Fig. 3, Table 3) revealed the lowest selectivity to acrolein. Two other samples (AuAg-SBA-15-A and AuAg-Zn/SBA-15-A) presented higher amount of silver in alloy, the highest for the sample containing zinc oxide, but the selectivity to acrolein was lower over AuAg-Zn/SBA-15-A than AuAg-SBA-15-A. A deeper insight into the UV-Vis spectra (Fig. S10-SD) allowed the

observation of differences in absorbance line slopes suggesting differences in the number of alloy NPs formed (lower number on AuAg-Zn/SBA-15-A). As documented in section 3.3.4., zinc species interacted with metallic silver. Such interaction could lower the number of alloy NPs formed, which caused a lower selectivity to acrolein.

The treatment of the catalysts with hydrogen flow before the reaction led to an increase in activity of AuAg-Zn/SBA-15-H and AuAg-SBA-15-H samples (from 4 to 7% and 3 to 9% of propene conversion at 573 K, respectively) (Table 5). This behaviour was not observed for bimetallic AuAg-ZnO-H sample. Surprisingly, selectivity to acrolein was lower over the bimetallic samples reduced before the reaction than over the catalysts only activated in inert gas flow, although hydrogen treatment made the Au-Ag alloy richer in silver. To explain this phenomenon, the UV-Vis spectra were measured for the catalysts after propene oxidation (Fig. S11-SD). Table 3 presents the positions of the SPR band characteristic of Au-Ag alloy. In the case of alloy formed after catalyst activation in the inert gas flow, the SPR band after the reaction was red shifted by 6 nm for AuAg-ZnO-A and AuAg-SBA-15-A and 3 nm for AuAg-Zn/SBA-15-A. The red shift observed indicated partial segregation of metals in the alloy. This segregation was much greater over the catalysts hydrogen treated before the reaction (red shift of 11 nm – 25 nm, depending on the catalyst). That is why the selectivity to acrolein was lower over these catalysts than over the materials activated only in the inert gas. The easy segregation of the alloy enriched in silver leads to generation of metallic silver [43] which is responsible for the activity and total oxidation of propene. Partial separation of metals from PtAg alloy has been found earlier for bimetallic PtAg-MCF samples activated in argon and hydrogen [43] and then used in propene oxidation.

The segregation of metals in the alloy was confirmed by XANES spectra (Fig. S3-SD). The shapes of the XANES spectra obtained for AuAg-SBA-15-HR and AuAg-Zn/SBA-15-HR after the reaction do not differ very much from those of the spectra of calcined

catalysts. It indicates partial separation of Au-Ag alloy on the surface of mesoporous catalysts.

3.4.2. Methanol oxidation with molecular oxygen

The catalysts were also tested in oxidation of methanol (MeOH) in the gas phase. Methanol is one of the most important feedstock in the chemical industry and formaldehyde (FA), methyl formate (MF) and methylal are the main products of its selective oxidation [44]. The results of methanol oxidation are presented in Table S1-SD and Fig. 7.

SBA-15 was inactive in methanol oxidation in the conditions used. The activity of the supports containing zinc was very low (Table S1-SD) and observed only at higher reaction temperatures. However, the selectivity of the reaction over zinc containing supports allowed us to characterize their surface properties. It is clear that Zn/SBA-15 revealed acidic properties concluded from high selectivity to dimethyl ether and ethane formed on acidic centres in intermolecular dehydration [45], whereas ZnO presented redox activity combined with the participation of acidic centres (methyl formate as the main reaction product [46]).

Loading of gold on the supports (ZnO, SBA-15 and Zn/SBA-15) and activation of the catalysts in the inert gas flow at 673 K before the reaction generated high activity in MeOH oxidation. It is clear that gold is responsible for the catalyst activity (almost total conversion of MeOH at 473-523 K). The results are in good agreement with literature reports showing high activity of Au loaded on metal oxides in selective methanol oxidation [9,47,48]. The effect of zinc on the catalyst activity was not observed. It is in line with the fact that only the interactions between cationic gold and zinc were found in bimetallic samples, whereas $(\text{Au}^0)^\delta$ species are active in methanol oxidation [37]. The MeOH conversion on Au-SBA-15-A and Au-Zn/SBA-15-A was high and very similar in the range of 423-523 K. It is important to stress that the average gold particle sizes did not differ in both samples (Table 2). However, the Au particle size is not the only parameter that would influence the activity. The role of the

size of metal particles can be analysed on the basis of the results obtained at lower reaction temperature (5% vs 83% of MeOH conversion over Au-ZnO-A and Au-Zn/SBA-15-A at 423 K). The activities of both Au-catalysts were calculated as the number of MeOH molecules that reacted per minute per 1 nm² of the surface area of gold crystallites. The activity of Au-ZnO-A was significantly lower than that of Au-Zn/SBA-15-A in spite of smaller gold particles on Au-ZnO (TOF = 39 vs 977 [mmol of MeOH molecules/min/nm²] over Au-ZnO-A and Au-Zn/SBA-15-A, respectively). This evidences the role of the nature of the support. ZnO seems to take part in the reaction steps in methanol oxidation [46]. These steps cover dissociative chemisorption of methanol (methoxy species are chemisorbed on acidic sites), dehydrogenation of methoxy species to formaldehyde and possibly the following transformations of FA and reactions with other MeOH molecules, if FA is relatively strongly chemisorbed, so that finally total oxidation can occur (the rake reaction mechanism). The role of the support composition is expressed by high selectivity to methyl formate over zinc containing samples, which requires relatively strong chemisorption of formaldehyde (the first product in step by step oxidation of methanol) on Lewis acid sites (coming from cationic gold and ZnO) that allows the further reaction with another MeOH molecule. The 100 % selectivity to MF was achieved over Au-ZnO at 423 K with low methanol conversion (5 %). Such a low conversion can be related to very low surface area of this catalyst, which became less important at higher reaction temperatures (473 K and 523 K). The role of zinc species in the production of MF is well expressed in Fig. 7 showing the selectivity over two catalysts, Au-SBA-15 and Au-Zn/SBA-15, at 423 K, with almost the same methanol conversion (85 % and 83 %, respectively). The presence of zinc enhanced the selectivity to MF from 47 % to 66 % and reduced the total oxidation of methanol to CO₂. At higher reaction temperatures, the activity of most catalysts was very high (above 90 % of methanol conversion). Therefore, in further consideration the lower reaction temperatures (373 K and 423 K) are mostly taken into

account. Generally, the selectivity to formaldehyde increased with increasing temperature, whereas the selectivity to methyl formate decreased at the same sequence, which is in line with literature data [49].

Silver catalysts were less active than gold ones (especially at higher reaction temperatures) and the main reaction product was methyl formate, which can be explained by a significant amount of cationic silver (Table 4), playing the role of Lewis acid sites.

The bimetallic catalysts activated in the inert gas flow before the reaction, presented significantly higher activity. This effect is well visible at lower reaction temperatures. It was accompanied by the increase in total oxidation of methanol to CO₂, that is illustrated in Fig. 7 plotted for the same reaction temperature and the same conversion of methanol. However, the effect of zinc species which took part in selective oxidation to methyl formate is also visible (AuAg-SBA-15-A vs AuAg-Zn/SBA-15-A - Table S1-SD). Moreover, Fig. 7 shows higher selectivity to FA over AuAg-ZnO-A than over AuAg-Zn/SBA-15-A which is in line with a lower acidity of the former sample.

Activation of the bimetallic catalysts in hydrogen flow significantly decreased methanol conversion at lower reaction temperatures (Table S1-SD). Both zinc containing samples treated with hydrogen were inactive at 373 K and 423 K. As mentioned in the characterization section, the hydrogen treatment caused the enrichment of Au-Ag alloy in silver. Thus, the observed decrease in activity indicates that the alloy was not the active species in methanol oxidation. Therefore, the increase in methanol conversion over bimetallic samples with respect to monometallic catalysts was not due to the alloy formation but rather to the changes in composition of gold species (increase in (Au⁰)^{σ-} and decrease in Au^{σ+}) upon introduction of silver (Table 4). The increase in the number of active metallic negatively charged gold, accompanied by the decrease in the number of cationic gold species, resulted in enhancement of activity and decrease in selectivity to FA and MF.

The alloy stability during methanol oxidation was much higher than that observed in propene oxidation (Table 3) in spite of the fact that in both reactions O_2 was used as a reagent. Very small red and blue shifts in the position of the SPR UV-Vis band characteristic of gold-silver alloy, resulted from two opposite actions, oxidation conditions conducive to separation of metals in the alloy and reductive (reduction by formaldehyde – the reaction product) atmosphere inducing alloy formation.

4. Conclusions

The thermal treatment of bimetallic AuAg-containing materials in inert gas flow at 673 K led to the formation of Au-Ag alloy. The number of alloy NPs was limited by the presence of ZnO. The Au-Ag alloy was enriched in silver by the reduction with hydrogen at 673 K. The presence of zinc in the support (Zn/SBA-15, ZnO) favoured deeper alloying of gold and silver under reduction conditions, but did not affect too much the alloying upon treatment in the inert gas. The enrichment of the alloy in silver decreased in the following order: AuAg-Zn/SBA-15-H > AuAg-ZnO-H > AuAg-SBA-15-H. The strong interaction of small ZnO particles loaded on SBA-15 with metallic species, resulted in deeper alloying of gold and silver. The $(Au^0)^{\delta-}$ metallic particles dominated in AuAg-Zn/SBA-15 and AuAg-ZnO samples, but cationic gold was also present. Zinc species interacted with silver species and cationic gold, but not with metallic gold.

As concerns the catalytic activity, silver species were responsible for the activity in propene total oxidation on mono- and bimetallic catalysts. Gold showed very low activity in this reaction. The addition of silver to gold and the presence of Au-Ag alloy favoured the activity and selectivity to acrolein. The highest selectivity to acrolein was achieved over AuAg-SBA-15-A, not over the samples containing the alloy rich in silver (e.g. AuAg-

Zn/SBA-15-H) because the silver reached alloy was easily separated onto both metals in the reaction conditions.

In methanol oxidation gold (Au^0)^{δ-} was responsible for the activity of mono- and bimetallic catalysts. Silver catalysts were less active. The addition of silver to gold increased the activity of catalysts at low reaction temperatures as a result of the increase in the number of negatively charged metallic gold particles. The presence of zinc in the matrix did not influence the activity, but it affected the selectivity at lower reaction temperature (473 K). Stronger adsorption of formaldehyde on the samples containing zinc allowed further reaction with the second methanol molecule, leading to higher selectivity to methyl formate. The addition of silver to gold increased the total oxidation of MeOH to CO₂. Formaldehyde was stronger chemisorbed on the surface of bimetallic catalysts (chemisorption on metal cations) allowing further reactions with the formation of CO₂ in the last step of the rake mechanism.

Acknowledgements

“EURASIACAT: Advanced Education European-Asiatic Exchange Program in Materials Science and Catalysis” and National Science Centre in Poland (Grant No. 2013/10/E/ST5/00642) are acknowledged for the financial support of this work.

C.M.Y. also gratefully acknowledges the financial supports of the Ministry of Science and Technology, Taiwan under the contracts No. MOST 106-2113-M-007-025-MY3 and MOST 107-3017-F-007-002 and The Frontier Research Centre on Fundamental and Applied Sciences of Matters from The Featured Areas Research Centre Program within the framework of the Higher Education Sprout Project by the Ministry of Education (MOE) in Taiwan. The authors wish to thank the National Synchrotron Radiation Research Center (NSRRC) of Taiwan for XAS measurements.

References

- [1] X. Liu, A. Wang, T. Zhang, D.S. Sub, Ch.Y. Mou, *Catal. Today* 160 (2011) 103–108
- [2] A. Wang, X. Y. Liu, Ch.Y. Mou, T. Zhang, *J. Catal.* 308 (2013) 258–271
- [3] X.Y. Liua, A. Wang, T. Zhang, Ch.Y. Mou, *Nano Today* 8 (2013) 403–416
- [4] L. Wolski, I. Sobczak, M. Ziolk, *Micropor. Mesopor. Mat.* 243 (2017) 339–350
- [5] A.Q. Wang, Ch.M. Chang, Ch.Y. Mou, *J. Phys. Chem. B* 109 (2005) 18860–18867
- [6] S. Belin, Ch.L. Bracey, V. Briois, P.R. Ellis, G.J. Hutchings, T.I. Hyde, G. Sankar, *Catal. Sci. Technol.* 3 (2013) 2944–2957
- [7] Ch.L. Bracey, A.F. Carley, J.K. Edwards, P.R. Ellis, G.J. Hutchings, *Catal. Sci. Technol.* 1 (2011) 76–85
- [8] F.W. Zemichael, A. Al-Musa, I.W. Cumming, K. Hellgardt, *Sol. St. Ionics* 179 (2008) 1401–1404
- [9] I. Sobczak, E. Dembowski, *J. Mol. Catal. A: Chemical* 409 (2015) 137–148
- [10] I. Bilkova, I. Sobczak, P. Decyk, M. Ziolk, J.E. Whitten, *Micropor. Mesopor. Mater.* 232 (2016) 97–108
- [11] A. Senthilraja, B. Subash, B. Krishnakumar, D. Rajamanickam, M. Swaminathan, M. Shanthi, *Mat. Sci. Sem. Proces.* 22 (2014) 83–91
- [12] X. Liu, M.H. Liu, Y.Ch. Luo, Ch.Y. Mou, S.D. Lin, H. Cheng, J.M. Chen, J.F. Lee, T.S. Lin, *J. Am. Chem. Soc.* 134 (2012) 10251–10258
- [13] S. Sareen, V. Mutreja, S. Singha, B. Pal, *RSC Adv.* 5 (2015) 5 184–190
- [14] S.Y. Chen, Y.T. Chen, J.J. Leec, S. Cheng, *J. Mater. Chem.* 21 (2011) 5693–5703
- [15] S.Y. Chen, Ch.Y. Tang, W.T. Chuang, J.J. Lee, Y.L. Tsai, J.C.C. Chan, Ch.Y. Lin, Y.Ch. Liu, S. Cheng, *Chem. Mater.* 20 (2008) 3906–3916
- [16] L. Wolski, J.E. Whitten, I. Sobczak, M. Ziolk, *Mat. Res. Bull.* 85 (2017) 35–46
- [17] P.H. Ku, Ch.Y. Hsiao, M.J. Chen, T.H. Lin, Y.T. Li, S.Ch. Liu, K.T. Tang, D.J. Yao, Ch.M. Yang, *Langmuir* 28 (2012) 11639–11645

- [18] X. Liu, A. Wang, X. Yang, T. Zhang, Ch.Y. Mou, D-S. Su, J. Li, *Chem. Mater.* 21 (2009) 410–418
- [19] P. Fageria, S. Gangopadhyay, S. Pande, *RSC Adv.* 4 (2014) 24962–24972
- [20] A. Moosavi, M. Sarrafi, A. Aghaei, F.A. Hessari, M. Keyanpour-Rad, *Micro & Nano Letters* 7 (2012) 130–133
- [21] Y. Tai, A. Shaporenko, H.T. Rong, M. Buck, W. Eck, M. Grunze, M. Zharnikov, *J. Phys. Chem. B* 108 (2004) 16806–16810
- [22] H. Yazid, R. Adnan, S.A. Hamid, M. A. Farrukh, *J. Chem.* 34 (2010), 639–650
- [23] I. Kaskow, P. Decyk, I. Sobczak, *Appl. Surf. Sci.* 444 (2018) 197–207
- [24] Z.H. Dhoondia, H. Chakraborty, *Nanomater. Nanotechnol.* 2 (2012) 1–7
- [25] A.Q. Wang, J.H. Liu, S.D. Lin, T.S. Lin, Ch.Y. Mou, *J. Catal.* 233 (2005) 186–197
- [26] Z. Qu, G. Ke, Y. Wang, M. Liu, T. Jiang, J. Gao, *Appl. Surf. Sci.* 277 (2013) 293–301
- [27] S.S. Kumar, P. Venkateswarlu, V.R. Rao, G.N. Rao, *Int. Nano Letters* 3 (2013) 30–35
- [28] D.L. Feldheim, C.A. Foss, *Metal nanoparticles. Synthesis, characterization and applications*, Basel, Marsel Dekker, Inc., New York, 2002
- [29] S.W. Han, Y. Kim, K. Kim, *J. Coll. Interf. Sci.* 208 (1998) 272–278
- [30] T. Benkó, A. Becka, K. Freya, D.F. Srankóá, O. Geszti, G. Sáfrán, B. Maróti, Z. Schay, *Appl. Catal. A: General* 479 (2014) 103–111
- [31] I. Tuzovskaya, N. Bogdanchikova, A. Simakov, V. Gurin, A. Pestryakov, M. Avalos, M.H. Farias, *Chem. Mater.* 20 (2008) 3906–3916
- [32] S. Link, M. A. El-Sayed, *Int. Rev. Phys. Chem.* 19 (2000) 409–453
- [33] J. Radnik, Ch. Mohr, P. Claus, *Phys. Chem. Chem. Phys.* 5 (2003) 172–177

- [34] A.M. Venezia, G. Pantaleo, A. Longo, G. Di Carlo, M.P. Casaletto, F.L. Liotta, G. Deganello, *J. Phys. Chem. B* 109 (2005) 2821–2827
- [35] P. Lignier, M. Comotti, F. Schuth, J-L. Rousset, V. Caps, *Catal. Today* 141 (2009) 355–360
- [36] S. Albonetti, T. Pasini, A. Lolli, M. Blosi, M. Piccinini, N. Dimitratos, J.A. Lopez-Sanchez, David J. Morgan, A.F. Carley, G.J. Hutchings, F. Cavani, *Catal. Today* 195 (2012) 120–126
- [37] L. Wolski, I. Sobczak, M. Ziolek, *J. Catal.* 354 (2017) 100–112
- [38] M.P. Casaletto, A. Longo, A. Martorana, A. Prestianni, A.M. Venezia, *Surf. Interface Anal.* 38 (2006) 215–218
- [39] Ch. Wang, S. Peng, R. Chan, S. Sun, *Small* 5 (2009) 567–570
- [40] F.W. Chang, S.C. Lai, L.S. Roselin, *J. Mol. Catal. A* 282 (2008) 129–135
- [41] J.H. Liu, A.Q. Wang, Y.S. Chi, H.P. Lin, Ch.Y. Mou, *J. Phys. Chem. B* 109 (2005) 40–43
- [42] Z.M. Hu, H. Nakai, H. Nakatsuji, *Surf. Sci.* 401 (1998) 371–391
- [43] J. Wisniewska, Ch.M. Yang, M. Ziolek, *Catal. Today* (2018), in press, doi: 10.1016/j.cattod.2018.03.001
- [44] C.H. Bartholomew, R.J. Farrauto, *Fundamentals of Industrial Catalysis Processes*, John-Wiley & Sons. Inc, 2005
- [45] J.M. Tatibouet, *Appl. Catal. A: General* 148 (1997) 213–252
- [46] G. Busca, A.S. Elmi, P. Forzatti, *J. Phys. Chem.* 91 (1987) 5263–5269
- [47] K. Kähler, M.C. Holz, M. Rohe, A.C. van Veen, M. Muhler, *J. Catal.* 299 (2013) 162–170
- [48] S. Velu, L. Wang, M. Okazaki, K. Suzuki, S. Tomura, *Micropor. Mesopor. Mat.* 54 (2002) 113–126

[49] I. Sobczak, *Cat. Today* 142 (2009) 258–266

ACCEPTED MANUSCRIPT

Captions to figures

Fig. 1. XRD patterns of ZnO (A), Zn/SBA-15 and SBA-15 (B) supports.

Fig. 2. XRD patterns of mono- and bimetallic catalysts based on ZnO (A), SBA-15 (B) and Zn/SBA-15 (C).

Fig. 3. UV-Vis spectra of mono- and bimetallic catalysts based on ZnO (A), SBA-15 (B) and Zn/SBA-15 (C) (in symbol of catalysts: A - samples activated in the inert gas flow, H - samples activated in hydrogen flow).

Fig. 4. Metal particle size distribution for calcined mono- and bimetallic materials supported on ZnO, SBA-15 and Zn/SBA-15.

Fig. 5. Metal particle size distribution for reduced bimetallic materials supported on ZnO, SBA-15 and Zn/SBA-15.

Fig. 6. Selectivity of gold-containing catalysts in propene oxidation with O₂ at 573 K – the effect of silver (A) and zinc (B) (Others: methane, propene oxide, ethanol, propanal, acetone).

Fig. 7. Selectivity of mono- and bimetallic catalysts in methanol oxidation with O₂ at 423 K for the same range of activity (83%-85% of methanol conversion).

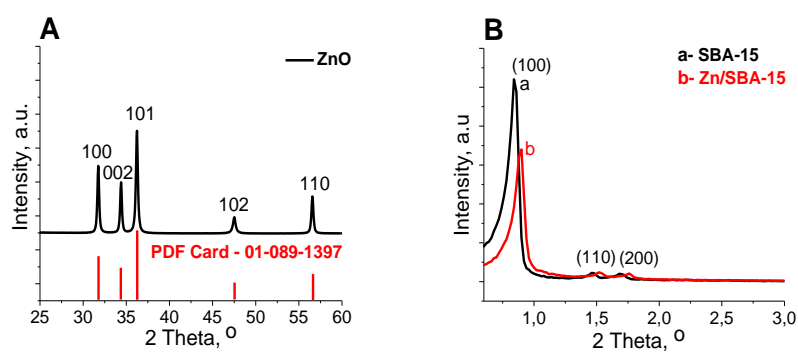


Fig. 1. XRD patterns of ZnO (A), Zn/SBA-15 and SBA-15 (B) supports.

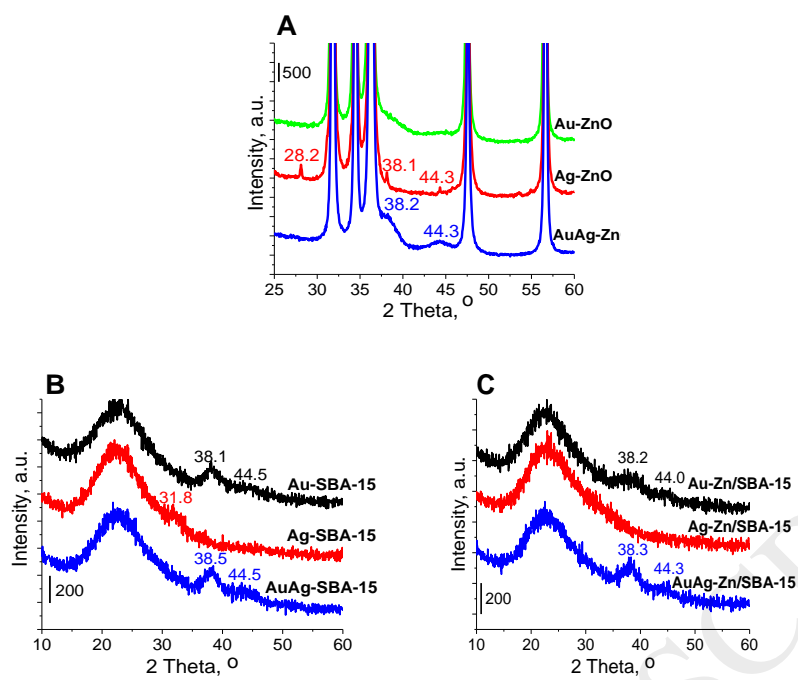


Fig. 2. XRD patterns of mono- and bimetallic catalysts based on ZnO (A), SBA-15 (B) and Zn/SBA-15 (C).

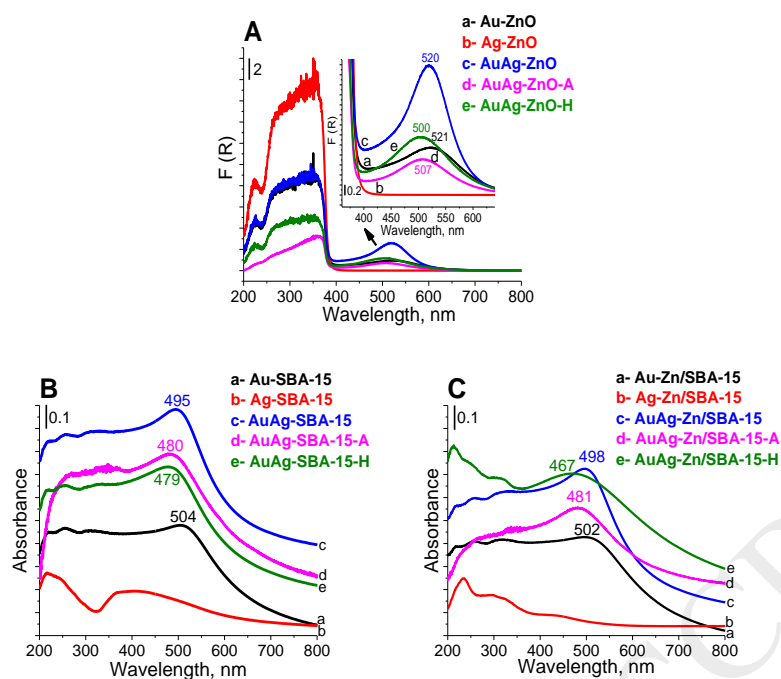
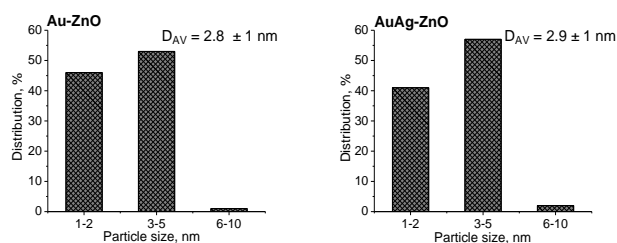


Fig. 3. UV-Vis spectra of mono- and bimetallic catalysts based on ZnO (A), SBA-15 (B) and Zn/SBA-15 (C) (in symbol of catalysts: A - samples activated in the inert gas flow, H - samples activated in hydrogen flow).



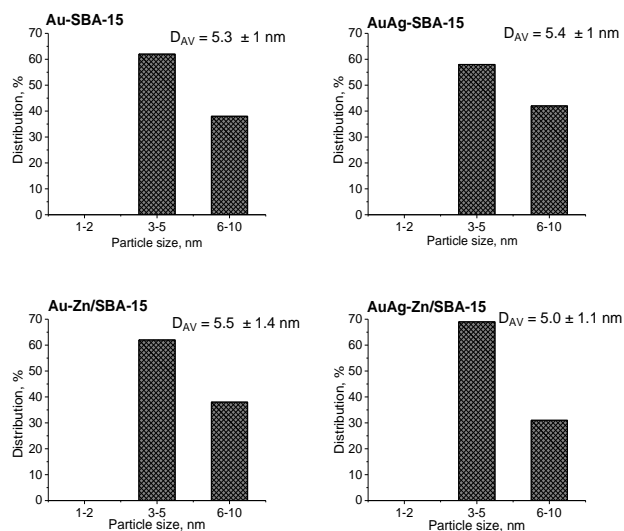
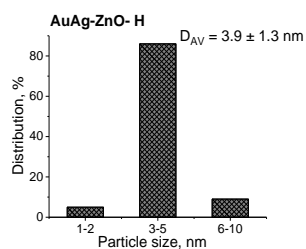


Fig. 4. Metal particle size distribution for calcined mono- and bimetallic materials supported on ZnO, SBA-15 and Zn/SBA-15.



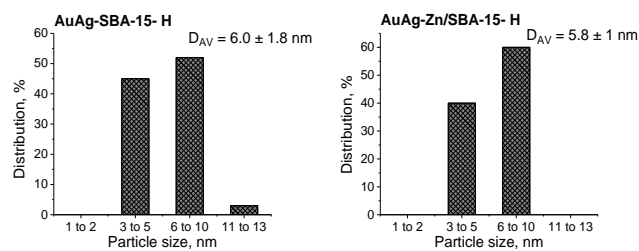
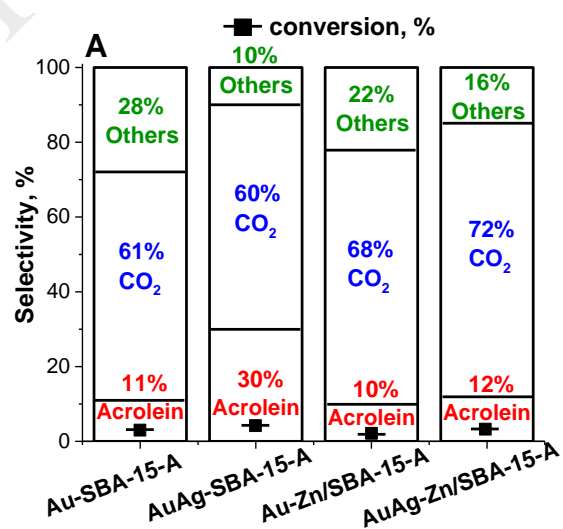


Fig. 5. Metal particle size distribution for reduced bimetallic materials supported on ZnO, SBA-15 and Zn/SBA-15.



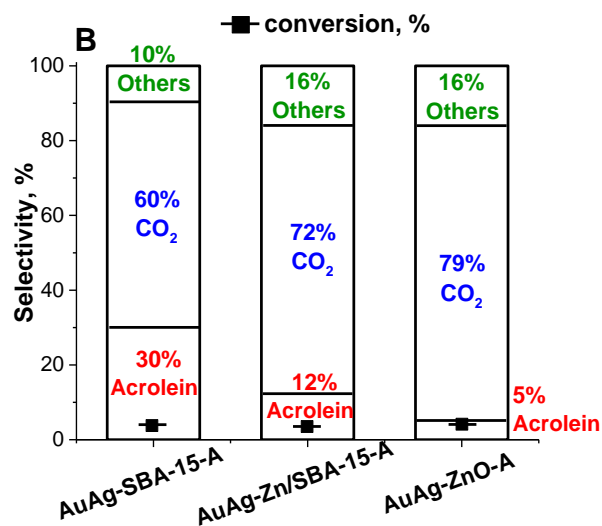


Fig. 6. Selectivity of gold-containing catalysts in propene oxidation with O₂ at 573 K – the effect of silver (A) and zinc (B) (Others: methane, propene oxide, ethanol, propanal, acetone).

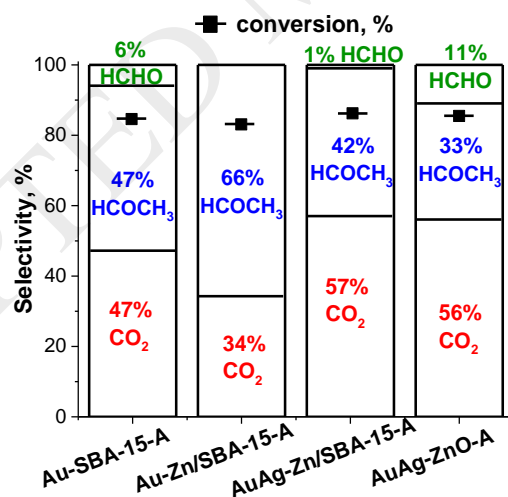


Fig. 7. Selectivity of mono- and bimetallic catalysts in methanol oxidation with O₂ at 423 K for the same range of activity (83%-85% of methanol conversion).

ACCEPTED MANUSCRIPT

Table 1. Textural properties of the materials prepared in this study.

Sample	BET surface area, m ² /g	Pore volume ^a , cm ³ /g	Average pore diameter ^a , nm
ZnO	18	0.13	30.5
Au-ZnO	18	0.14	29.8
Ag-ZnO	17	0.15	30.1
AuAg-ZnO	17	0.13	28.8
SBA-15	680	0.88	7.4
Au-SBA-15	513	0.85	7.5
Ag-SBA-15	373	0.77	7.4
AuAg-SBA-15	505	0.85	7.2
Zn/SBA-15	348	0.61	6.5
Au-Zn/SBA-15	308	0.55	6.6
Ag-Zn/SBA-15	301	0.55	6.5
AuAg-Zn/SBA-15	312	0.57	6.6

^a Determined from the adsorption branches by using the BJH method.

Table 2. Metals loading in the catalysts and the size of metal crystallites^a.

Catalyst	Au, wt. %	Ag, wt. %	Zn, wt. %	Average gold crystallite size- calcined samples, nm	Average metal crystallite size- reduced samples, nm
Au-ZnO	2.2	-	-	2.8 ± 1.0	-
Ag-ZnO	-	0.7	-	-	-
AuAg-ZnO	2.2	0.7	-	2.9 ± 1.0	3.9 ± 1.3
Zn/SBA-15	-	-	6.0	-	-
Au-SBA-15	1.6	-	-	5.3 ± 1.0	-
Ag-SBA-15	-	2.0	-	-	-
AuAg-SBA-15	1.4	0.5	-	5.4 ± 1.0	6.0 ± 1.8
Au-Zn/SBA-15	1.9	-	5.3	5.5 ± 1.4	-
Ag-Zn/SBA-15	-	1.9	5.6	-	-

AuAg-Zn/SBA-15	1.8	0.5	5.3	5.0 ± 1.1	5.8 ± 1.0
----------------	-----	-----	-----	---------------	---------------

^a Metal loadings were determined by ICP-MS and the metal crystalline sizes were measured by TEM.

ACCEPTED MANUSCRIPT

Table 3. Positions of SPR bands in the UV-Vis spectra of selected samples.

Catalyst	After calcination	After activation in the inert gas	After propene oxidation	After methanol oxidation	After activation in hydrogen	After propene oxidation	After methanol oxidation
AuAg-ZnO	520 nm	507 nm	513 nm	504 nm	500 nm	525 nm	502 nm
AuAg-SBA-15	495 nm	480 nm	486 nm	486 nm	479 nm	490 nm	478 nm
AuAg-Zn/SBA-15	498 nm	481 nm	484 nm	478 nm	467 nm	485 nm	476 nm

ACCEPTED MANUSCRIPT

Table 4. XPS results for catalysts studied.

Catalyst	Au 4f _{7/2}			Ag 3d _{5/2}			Zn	
	BE, eV	Species	%	BE, eV	Species	%	BE, eV	Species
ZnO	-	-	-	-	-	-	1022.0	-
Au-ZnO	83.2	(Au ⁰) ^{δ-}	70	-	-	-	1021.5	Zn ²⁺
	85.0	Au ^{δ+}	30	-	-	-	-	-
Ag-ZnO	-	-	-	368.4	Ag ⁰	43	1021.6	Zn ²⁺
	-	-	-	367.5	Ag ⁺	57	-	-
AuAg-ZnO	83.2	(Au ⁰) ^{δ-}	73	368.5	Ag ⁰	22	1021.8	Zn ²⁺
	84.9	Au ^{δ+}	27	367.3	Ag ⁺	78	-	-
Au-SBA-15	83.3	(Au ⁰) ^{δ-}	83	-	-	-	-	-
	84.6	Au ^{β+}	17	-	-	-	-	-
Ag-SBA-15	-	-	-	368.3	Ag ⁰	38	-	-
	-	-	-	367.7	Ag ⁺	62	-	-
AuAg-SBA-15	83.3	(Au ⁰) ^{δ-}	100	368.3	Ag ⁰	17	-	-
	-	-	-	367.5	Ag ⁺	83	-	-
Zn/SBA-15	-	-	-	-	-	-	1022.9	Zn ²⁺
Au-Zn/SBA-15	83.3	(Au ⁰) ^{δ-}	87	-	-	-	1022.4	Zn ²⁺
	85.4	Au ^{δ+}	13	-	-	-	-	-
Ag-Zn/SBA-15	-	-	-	368.3	Ag ⁰	39	1022.3	Zn ²⁺
	-	-	-	367.7	Ag ⁺	61	-	-
AuAg-Zn/SBA-15	83.2	(Au ⁰) ^{δ-}	92	368.3	Ag ⁰	16	1022.3	Zn ²⁺

85.3	$\text{Au}^{\delta+}$	8	367.4	Ag^+	84
------	-----------------------	---	-------	---------------	----

ACCEPTED MANUSCRIPT

Table 5. Activity and selectivity of catalysts in propene oxidation with O₂.

Catalyst	523 K				573 K			
	Conv., %	Select. to acrolein, %	Select. to CO ₂ , %	Others*, %	Conv. %	Select. to acrolein, %	Select. to CO ₂ , %	Others*, %
Au-ZnO-A	0	-	-	-	<1	traces	traces	traces
Ag-ZnO-A	2	1	92	7	10	traces	92	~ 8
AuAg-ZnO-A	1	20	61	19	4	5	77	18
AuAg-ZnO-H	1	16	56	28	3	4	76	20
Au-SBA-15-A	1	11	50	39	3	11	61	28
Ag-SBA-15-A	4	1	89	10	17	traces	92	~ 8
AuAg-SBA-15-A	1	51	35	14	4	30	60	10
AuAg-SBA-15-H	2	32	55	13	7	14	72	14
Au-Zn/SBA-15-A	0	-	-	-	2	10	68	22
Ag-Zn/SBA-15-A	5	1	87	12	18	traces	90	~ 10
AuAg- Zn/SBA-15-A	1	33	50	17	3	12	72	16
AuAg- Zn/SBA-15-H	2	8	74	18	9	2	82	16

* Others: methane, ethanal, propene oxide, propanal, acetone

A- samples activated in the flow of inert gas at 673 K

H – samples activated in hydrogen flow at 673 K

ACCEPTED MANUSCRIPT